ISSN: 2366-1313

PROPERTIES OF THE STRUCTURAL, MAGNETIC, AND MAGNETOCALIBRI COMPOSITES CONTAIN CRYSTAL FIELD INTERACTIONS.

Rachuri Venkataiah, Research Scholar, Department of Physics , Radha Govind University, Ramgarh,Jharkhand.
Dr. Sachin Saxena ,Assistant Professor ,Supervisor, Department of Physics ,Radha Govind University, Ramgarh,Jharkhand.

Abstract: Since electrical insulations are devoid of conduction electrons, they provide the opportunity to examine the effects of magnetic interaction. Studies on different dimerized antiferro magnets that are insulating have shown the concave-down phenomenon of magnetic susceptibility during the last 10 years at magnetic fields larger than a certain threshold. The phenomenon is difficult to understand. When the magnetic field increased over the critical threshold, certain characteristics of the anomaly lambda's residual heat capacity related to the super fluid transition in liquid 4He could be seen. These results are connected to long-range magnetic order, or Bose-Einstein condensation (BEC) in the situation of indeterminate spin excitations, commonly known as magnons. Although technically not a BEC, magnons are believed to fit the BEC definition very well in order to explain some of the reported values of the small number of insulating antiferro magnets that exhibit the field-induced concave-down susceptibility at low temperatures. One of the systems that exhibits this concave-down and low temperature sensitivity to magnetic fields due to a field is Pb2V3O9, which is mentioned in this BEC description.

Keywords : Magnetic, Crystal, and Composites

I Introduction

The easy direction, or the easy axis is a particular crystallographic orientation that is typically kept by anisotropy energy [1]. The location where the magnetic field will naturally be in the absence of any external force is decided through the simple direction. The anisotropy constant Ku that is inherent to the material plays an important role to play in determining

ISSN: 2366-1313

the direction. The magnetic moments are controlled in a specific direction by magnetic anisotropy energy. Since the energy of thermal of kBT corresponds to the anisotropy power that creates the energy barrier known as KuV, which separates the two equally energetic directions of magnetization, at 0. (parallel) as well as = (antiparallel) in super paramagnetic particles The magnetization reverses itself spontaneously and [2,3]. If the energy of the thermal is greater than KuV's energy threshold and the magnetic field of single-domain, uniaxial super paramagnetic nano particles could spont aneously change in the event that T exceeds the blocking temperature of. Instead of atomic magnets that are above TB, this system acts as the paramagnet and every nanoparticle is now a massive amount of. The system is devoid of the phenomenon of hysteresis. The orientation of magnetizations varies. The frequency of f, or the normal relaxation time determines the fluctuations in magnetization.

For the sake of simplicity, it is often believed that the relaxation period of a nano particle's moment has a constant value between 10-9 and 10-13 s [4]. As the sample cools to lower temperatures, the fluctuations grow slower (rises), and the system seems static when exceeds the experimental measurement period m. Some m [5] characteristic values are collected in Table III. A magnetism will seem to be "blocked" (unable to move) if the time m is less than the relaxation time, as opposed to a "unblocked" magnet-ization, which is characteristic of a nano particle in the super paramagnetic domain.

Table 1. Measurement times for various magnetic measurement methods

Techniques	Measurement Time τ_m[s]
DC Susceptibility	60-100
AC Susceptibility	10^{2}-10^{4} (low frequency experiment) 10^{-1}-10^{-5} (classical experiment)
Mössbauer Spectroscopy	10^{-7}-10^{-9}
Ferromagnetic Resonance	10^{-9}
Neutron Diffraction	10^{-8}-10^{-12}
Magnetometer	100

The term "blocking temperature," often abbreviated TB is the temperature at which you can distinguish the super paramagnetic and the "blocked" system. In the scale of time measurements, m, nano particles' moments appear frozen beneath the temperature of TB. If m =, this is what happens. The anisotropy factor along with the particle's size and the applied magnetic field influence block temperature. The distribution of blocking temperatures is the result of the dispersion in nano particle size. Smaller particle sizes mean that the anisotropy Ku is increased. It is evident that the value for TB will be more significant when the

ISSN: 2366-1313

blocking temp is calculated by a method that has a smaller timeframe for example, ferromagnetic resonance with m = 10-9 seconds. This is due to the fact that the blocking temperature can be calculated by this technique. Contrary to the previous scenario, in which the magnetic field of the nano particle assembly is steady in the second, the nano particles assembly is super paramagnetic. It also does not have hysteresis. In addition, a double increase in size of the nano particles can decrease the time of reversal by 100 years, to a time of 100 nanoseconds.

II Literature Survey

Until recently, experimental research have mostly concentrated on dense arrays of similar components (stripes and dots) and antidot arrays, which are made of continuous ferromagnetic films with circular holes etched into them [6-7]. A few experimental studies have also focused on bicomponent magnetic crystals, which are composed of two distinct ferromagnetic materials in close proximity, such as cobalt and permalloy, or an arrangement of ferromagnetic rods embedded in another ferromagnet's matrix. We can categorise the two-dimensional magnonic crystals into three primary groups. They consist of bi component magnonic crystals, antidot lattices, and dot arrays. The first kind is made up of a regular arrangement of tiny ferromagnetic dots, whereas the second is a reflection of the first and is made up of a regular arrangement of tiny holes in ferromagnetic film. The final group may be thought of as a superposition of both, with antidot lattices filled with ferromagnetic material other than that used in the antidot lattices and having holes in them. The spin wave propagation of these three groupings has distinctive characteristics. The magneto static interaction between the spin wave modes that have been generated in each individual ferromagnetic dot in the array causes the dynamical coupling between the dots. The strength of coupling, which depends on the form of the dot and distance between dots, their arrangement in the lattices, as well as the configuration of their magnetic structure within a dot is determined by bandgap's width. The regularity of the magnetic field within the film plane is responsible for the formation of the magnonic band structure the in-plane antidot lattices that are magnetised. The inner magnetic field and shape of the magnonic band is also affected by the form and layout of the hole. Spin waves are susceptible scattering at the interfaces between two materials. They can be

ISSN: 2366-1313

transmitted through the surfaces of a two-dimensional bi component magnet, which comprises the regular configuration of two magnetic substances. The spin waves are subject to the field of demagnetization that is non-uniform that's magnitude is in inversely proportional to the magnitude of the saturation magnetizations of the constituent material. It is more difficult to create two-dimensional magnonic crystals. With the help of current technology, antidot periodic waveguides or magnonic crystals with a resolution of 10 nm may be created. With resolution in the hundreds of nanometer range, the creation of bicomponent planar magnonic crystals is more challenging but still possible.

The main difficulty with three-dimensional magnonic crystals is their production, particularly when the lattice constant is in the nano meter range. In general, top-down and bottom-up methods are used to construct these structures. Top down techniques include drilling holes in the bulk material (matrix) and filling them with inclusions made of a different magnetic substance. The goal of bottom-up approaches is to create the lattice of inclusions before adding the matrix to fill in the gaps. This opens the door to creating magnetic crystals in three dimensions using magnetic nano particles as a template. Magnonic band structure in magnonic crystals that are three dimensional. These studies give a comprehensive analysis of the impact of several variables on the magnonic band structure. Three-dimensional magnonic crystals were studied that were simple cubic faces-centered cube, body-centered and basic hexagonal crystallographic forms that took into consideration the structural parameters (filling percentage as well as lattice constant and an ellipsoidal deformation in the scattering centers) and magnetic properties of the components and the exchange constant. The magnonic spectrum as well as band gaps were mainly measured by the saturation magnetic contrast as well as the contrast between the exchange constant. If the value of the exchange constants in the components are similar the saturation magnetization contrast (periodic variation in the saturation magnetic intensity in the constituent material of magnonic crystal) at or above a particular minimum value in this periodic structure is a necessary conditions for the creation of magnonic bands to be become open. The crucial value of saturation magnetization contrast heavily depends on the lattice type. The gap's width can be significantly affected by exchange contrast, in absence of contrast in magnetization, this contrast

ISSN: 2366-1313

should be large to create the appearance gap gaps between magnonic bands.

III Methodology

The critical temperature for the use of REM is the temperature at which differences between the FM and PM order disappears or is the temperature when the FOPT's boundary changes into the boundaries of the SOPT. By definition, at T = Tcr, dHcr dT = 0. The presence of simultaneous three phases is essential for the formation of tricritical points, but the condition that the integral of the crucial parameter at or near zero temperatures is seldom met (the tricritical point in water is a unique case). The presence of tricritical points in diagrams of phase isn't overlooked due to the wide variety of magnetic phase transitions that occur in the heavy REM. In addition, a comparative study of the tricritical temperature in dysprosium with theoretical and actual values was observed in [8]. The authors note that although there is a theoretical figure of 168.4 K reported by the authors is more than the 165 K that was measured in [9] using samples of low quality, it's below the value measured in experiments of 172 K, which was reported in the exact same publication. At the same that, the magnetic diagram's line of division are a factor that influences the value that is measured by the tri-critical temperature. The measurements of the tri-critical temperature measurements requires particular recognition of three distinct phases with physical discernible boundaries since the accuracy that this technique provides isn't sufficient. As the transition from FM to the PM phase, or to a completely magnetic state Tb can be detected both with 236 K temperature, theoretical values of the terbium-tricritical point is not in line with the concept of a tricritical point. This should be noted that the tricritical region tends to occur within the region of helical AFM order or at its boundary with other phases of every other heavier REM. The discovery of the tricritical region in terbium is fascinating and difficult since the area is one of the most narrow within the heavy REM sequence. For heavy REM the transition PM-APM incorporates elements from first- and second-order phase transformations. The equation below for the temperature at which the material transforms from a magnetic state to an antiferromagnetic phase can be located in the molecular field models [10]:

The AFM-PM's transition temperature as well as the function of de Genne are in a functional one-to-one relationship for the

ISSN: 2366-1313

heavy REM one crystal. This could be due to the nature of the anti-ferromagnetic helical structure's temperature dependence on the angle of rotation (the angle between magnetic moments of neighbouring layer of magnetic material). When the value is low for this function, the amount of the rotation angle slight variations with temperature However, when G is increased, the alteration is more apparent as well, and after an optimum value it rapidly decreases until it is zero when a temperature is set. Similar to erbium it's been observed in [84] the magnetic field divides the Neel temperature of the case of holmium. This observation confirms the effects [11], that was discovered to occur in in REMs with a value on about four (holmium dysprosium and Terbium). The Ni1-xZnx, synthetic Fe2O4 (0.0 x 0.7) samples show the ferromagnetic-to-paramagnetic (FM-PM) transition as they increase in temperatures, as demonstrated by magnetic measurements dependent on temperature within the range of 50to 900 K, and a magnetic field that is 0.1 0.01 (Fig. 4). 4. Curie temperature, determined from M-T curves, and defined as the temperature that the dM/dT curve is compared to. T curve is at an absolute minimum. It is calculated at 845, 664 302. K, for an x value of 0.0, 0.3, 0.5, 0.5 and 0.7 for x = 0.0, 0.3, 0.5 and 0.7 (the deviations from the experimental data are lower than 1/10000). Figure 4.5 illustrates how magnetization and Curie temperature fluctuate as Zn concentration grows. The amount of Curie temperature, or TC decreases in a steady manner as zinc content increases. It is due to replacing magnetized Ni2+ ions, with magnetic Zn2+ions. Zn2+ions are thought to be found in the trihedral (A) site, but Ni2+ ions are more suited to the Octahedral (B) sites. Fe3+ ions can be found scattered between both sites

IV Experiments and Results

The most popular holotype of a class of metallic organic frameworks (MOFs) which can be able to concertina between closed and open pores through a process known as a "wine rack" deformation is MIL 53. Research is ongoing with these MOFs that are flexible to be used in gas separation and storage applications, as the transition from close and open configurations can trigger by absorption of gases or pressure. Conductivity in thermal form is often seen as the bottleneck in the dissipating of latent heat from the adsorption process, is an important part of the gas sorption efficiency of MOFs. In the letter that preceded we examined how the thermal

ISSN: 2366-1313

conductivity of MIL-53 varies from closed to open. In addition, we find out that although not changing as substantially as would be predicted based on the network's geometric shift, the thermal conductivity does vary considerably. We discover that the phonon concentrating effect, which is moderated by scattering from non-propagating "rattler" modes, is the cause of the thermal conductivity's anisotropy. The phonon transport community is very interested in the phenomenon of phonon focusing, which sheds important light on why MOFs as a class of materials are fundamentally bad at conducting heat due to their framework architecture.

Pb2V3O9 was subjected to X-Ray diffraction (XRD) experiments (see Experimental Methods Chapter) at FSU and the NHMFL in Tallahassee. Measurements on polycrystalline samples confirm the space group and the sample's quality.

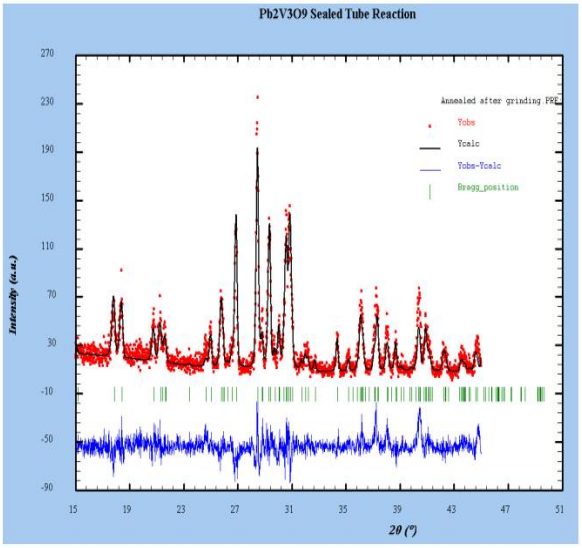

Figure .2 : XRD data for powder, . The black lines are computed, the blue curve depicts the difference, and the red spots are observed.

For the C 1 space group of Reference [16], Fig. 5.2 displays the computed intensity, difference, and raw XRD data (blue). The understanding is acceptable. The powder data fits quite well in either space group, however a C1 space group is more plausible, and refining yields almost the same unit cell. Tables 5.1 and 5.2 show the findings of twinned single crystal XRD studies. Information on Pb2V3O9's space group is shown in Table 5.1. With 28 atomic locations acting as variables, the refinement was carried out in a triclinic C1 space group. The findings are a space group that closely match earlier studies [16] [18]. C1 was chosen since it is a less arrogant option than the C 1. The table defines the R1 value, which is used to assess the "goodness of the fit." The structural factors are the F. The fit gives an acceptable value of R1 = 0.08 that is comparable in size to that of Mentre et al. (Ref. [18]). The V5+ site ambiguity and the twin refinement are potential causes of mistake. Table 5.2 shows the atomic locations for Pb2V3O9. Each of the first three columns' numbers represents a

ISSN: 2366-1313

portion of the unit cell's overall length in one direction. In the space for the location, the three integers constitute a vector. The atom's mean square displacement is shown in the final column, B. The spot's width is used to refine this number. Everything about the Pb2V3O9 crystals is quite well behaved, and the refinements will be taken as evidence of the single crystal quality. big B values often indicate poor crystalline samples and are typically coupled with big values of R1.

Table 2: Pb2V3O9 crystallographic data at 180 K

Space group	$C1$ (No. 1)
a (Å)	7.5853(5)
b (Å)	16.3476(8)
c (Å)	6.9647(5)
α (deg.)	91.539(5)
β (deg.)	119.312(7)
γ (deg.)	90.654(5)
V (Å^3)	752.49(8)
Z	4
$T(K)$	180
R_1	0.08

[a] $R_1 = \sum ||F_o|-|F_c|| / \sum |F_o|$

Table 3 : Positional Pb2V3O9 characteristics are shown in .

Atom	x	y	z	B (Å^2)
Pb1a	-0.0018	-0.123	0.22510	0.0153
Pb1b	-0.00407(16)	0.12242(6)	-0.21854(15)	0.0118(3)
Pb2a	0.01343(17)	0.45360(6)	0.25218(17)	0.0128(4)
Pb2b	-0.01442(20)	-0.45343(6)	-0.24647(18)	0.0191(5)
V1a	0.0080(6)	0.66033(23)	0.2605(6)	0.0094(5)
V1b	-0.0144(6)	-0.66040(22)	-0.2567(6)	0.0082(5)
V2a	-0.0153(7)	0.0809(3)	0.2647(7)	0.0136(6)
V2b	0.0013(5)	-0.08043(18)	-0.2557(5)	0.0039(4)
V3a	0.2831(6)	0.24379(25)	0.5375(6)	0.0109(6)
V3b	0.7825(6)	0.25799(25)	0.0366(6)	0.0099(5)
O1a	-0.503(3)	0.2133(11)	-0.230(3)	0.0121(5)
O1b	0.499(3)	-0.2147(11)	0.264(3)	0.0121(5)
O2a	0.111(3)	0.1470(11)	0.501(3)	0.0121(5)
O2b	-0.133(3)	-0.1432(11)	-0.496(3)	0.0121(5)
O3a	-0.159(3)	0.1380(11)	0.022(3)	0.0121(5)
O3b	0.168(3)	-0.1325(11)	-0.010(3)	0.0121(5)
O4a	0.147(3)	0.7299(11)	0.203(3)	0.0121(5)
O4b	-0.144(3)	-0.7369(11)	-0.210(3)	0.0121(5)

Measurement Results from Differential Scanning Calorimetry On the FSU campus, the TA Instruments Q600 machine was used to conduct high temperature Differential Scanning Calorimetry (DSC) measurements on ground single crystals of Pb2V3O9 (see Experimental Methods Chapter). The findings provide a more precise temperature measurement for the monoclinic-triclinic structural deformation shown in Reference [10]. The displacement of V5+ in the [11] chains explains this distortion. The raw C p(T) data from a DSC test in which Pb2V3O9 single crystals were heated to 800 K in an argon atmosphere are shown in Fig. 5.(a). The raw data has certain peculiar characteristics. When the machine is initially switched on, the first thing that stands out is the abrupt rise from 300 K to 320 K, followed by a constant rise up to 600 K, when C p(T) starts to fall. In

ISSN: 2366-1313

Figure 5.(b), a sharp feature at 759(1) K is seen.

Pb2V3O9's steep drop serves as the telltale evidence of a structural deformation. This was shown in Mentre et al.'s XRD peak splitting (Ref. [12]). Pb2V3O9 samples showed the XRD peak splitting, however Sr2V3O9 samples did not. It seems that compared to x-ray diffraction, where the transition temperature was unclear within a 100 K window, calorimetry allows for a more accurate estimate of the transition temperature. DSC does not provide a trustworthy high temperature C p(T) curve, at least not based on this data. When the machine was switched on, there was a sudden spike at 300 K, although this is probably definitely a false reading. Additionally, the reduction in C p(T) at 600 K is very dubious. The Dulong-Petit limit is the point at which the phonon contribution to the specific heat of a material approaches a temperature-independent constant. Pb2V3O9's high temperature C p(T) curve has not been published, and we skipped measuring it since doing so would take a lot of effort. I thus do not know how C p(T) behaves at high temperatures, but I do not think that the curve's form in Fig. 5.(a) is accurate.

Figure 5.: DSC measurement on Pb2V3O9 (a) raw data showing background curve across the whole temperature range. (b) A close-up of the spike characteristic that is connected to the structural deformation from the monoclinic to the triclinic phase.

Due to the difficulties of stabilising complicated 0structures with constant

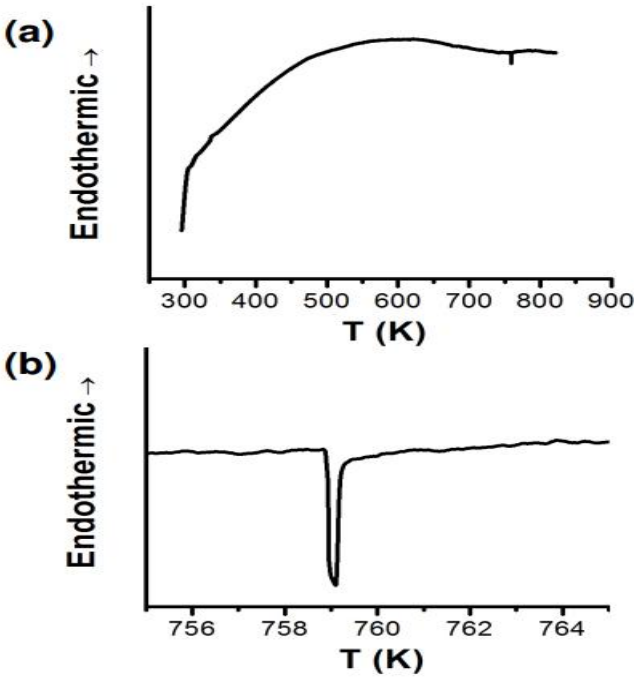

stoi-chiometry and the meta stability of the phases, osmium-containing oxides are uncommon. Tl2-xBixOs2O7-y samples of bismuth-substituted thallium osmate pyrochlore were made utilising solid state processes, and The limit of solubility was found to be in the region of the value of x

ISSN: 2366-1313

= 1.4. To understand how Bi3+ transformation alters the ground state elements of this solid solution were characterized according to their structure, magnetic, electrical, as well as thermal features. A perfect cubic pyrochlore crystallizes in the pyrochlores containing Os (Fd3 m) Then it was found that the lattice parameters slight increase in proportion to the degree of Bi's presence. By using neutron powder diffraction, as well as the X-ray absorption spectrum, a possible relationship between the structure as well as states of valence was examined. Results suggest that stabilization of the pyrochlore chain can be achieved through mixing different valency Tl1+/Tl3+ across the entire solid solution. The system shows temperature independent paramagnetism and is metallic throughout the whole solid solution. A putative flat-band signature may be seen in specific heat measurements, which indicate an elevated Sommerfeld coefficient. This system revealed information on the bonding preferences of Os, showing that the stability of complex structures depends on high oxidation states and mixed valence.

Table 5 : V5+-V5+ distances in various space groups.

Compound	Space group	Possible V^{4+}-V^{4+} distances (Å)	Source
$Sr_2V_3O_9$	C2/c	3.147; 3.651	Mentre et al.;1998[25]
$Pb_2V_3O_9$	C1	3.430; 3.457; 3.948; 3.962;	Mentre et al.;1999[16]
$Pb_2V_3O_9$	C1	3.688; 3.706	Mentre et al.;2008[18]
$Pb_2V_3O_9$	C1	3.677; 3.706	Conner et al.;2011[17]
$Pb_2V_3O_9$	Cc	3.700	Mentre et al.;2008[18]

Mentre et al. update their structure in Ref. [18], although it is impossible for the table of atomic locations they give to be accurate. I get improbable bond lengths and angles when I draw the structure according to what they describe in their database of atomic locations. However, Mentre et al. did report appropriate distances and angles in a different table in Ref. [18], therefore it is safe to believe that the atomic locations table contains mistakes and that the refinements were completed successfully at some point. Because it agrees with my own findings, the C1 space group will be taken as the actual space group. The relevant trade pathways will decide whether the degree of the distortion is important or not.

Magnetic susceptibility measurement results For sample verification and a study of the magnetic behaviour, magnetic susceptibility measurements as a function of temperature, (T), were made on ground single crystals of Pb2V3O9. The measurements were carried out at applied fields of 1T .

ISSN: 2366-1313

V Conclusion

The magnetization as a function of field, M(H), becomes finite for all non-zero fields when a little quantity of oxygen impurity creates a gap. In contrast, stoichiometric Pb2V3O9 possesses an energy gap under fields as big as 3 or 4 T, as was shown by Waki et al. in 2004 (Ref. [1]). A g value that is very close to 2 is obtained from EPR measurements. varying samples provide varying linewidths from EPR tests, some of which are shown to widen when the temperature is lowered. Similar to the C p(T) and (T), this provides more proof of potential glassy magnetic behaviour. The electrical resistivity of stoichiometric samples and samples with extra oxygen has been measured as a function of temperature. However, our Quantum Design PPMS cannot detect a big enough resistance to conduct measurements on manageable-sized samples. Resistivity measurements on samples with progressively more excess oxygen may reveal impurity effects on the band structure that cause Pb2V3O9 to degrade into a poor metal.

VI Reference

(1) Kim, J.-Y.; Kim, E.-R.; Han, Y.-K.; Nam, K.-H.; Ihm, D.-W. Highly Transparent Tin Oxide Films Prepared by DC Magnetron Sputtering and Its Liquid Crystal Display Application. Jap. J. Appl. Phys. 2002, 41, 237.

(2) Comini, E.; Faglia, G.; Sberveglieri, G.; Pan, Z.; Wang, Z. L. Stable and highly sensitive gas sensors based on semiconducting oxide nanobelts. Appl. Phys. Lett. 2002, 81, 1869– 1871.

(3) Snaith, H. J.; Ducati, C. SnO2-Based Dye-Sensitized Hybrid Solar Cells Exhibiting 18 Near Unity Absorbed Photon-to-Electron Conversion Efficiency. Nano Letters 2010, 10, 1259–1265.

(4) Ogale, S. B.; Choudhary, R. J.; Buban, J. P.; Lofland, S. E.; Shinde, S. R.; Kale, S. N.; Kulkarni, V. N.; Higgins, J.; Lanci, C.; Simpson, J. R.; Browning, N. D.; Das Sarma, S.;Drew, H. D.; Greene, R. L.; Venkatesan, T. High Temperature Ferromagnetism with a
Giant Magnetic Moment in Transparent Co-doped SnO2−δ. Phys. Rev. Lett. 2003, 91, 077205.

(5) Lussier, A.; Dvorak, J.; Idzerda, Y. U.; Ogale, S. B.; Shinde, S. R.; Choudary, R. J.; Venkatesan, T. Comparative x-ray absorption spectroscopy study of Co-doped SnO2 and TiO2. Journal of Applied Physics 2004, 95, 7190–7191.

(6) Hays, J.; Punnoose, A.; Baldner, R.; Engelhard, M. H.; Peloquin, J.; Reddy, K. M. Relationship between the structural and magnetic properties of Co-doped

ISSN: 2366-1313

SnO2 nanoparticles. Phys. Rev. B 2005, 72, 075203.

(7) Fitzgerald, C. B.; Venkatesan, M.; Dorneles, L. S.; Gunning, R.; Stamenov, P.; Coey, J. M. D.; Stampe, P. A.; Kennedy, R. J.; Moreira, E. C.; Sias, U. S. Magnetism in dilutemagnetic oxide thin films based on SnO2. Phys. Rev. B 2006, 74, 115307.

(8) Liu, X. F.; Sun, Y.; Yu, R. H. Role of oxygen vacancies in tuning magnetic propertiesof Co-doped SnO2 insulating films. Journal of Applied Physics 2007, 101, 123907.

(9) Zhang, J.; Skomski, R.; Yue, L. P.; Lu, Y. F.; Sellmyer, D. J. Structure and magnetism of V-doped SnO 2 thin films: effect of the substrate. Journal of Physics: Condensed Matter 2007, 19, 256204.

(10) Yu, W.; Jiang, K.; Wu, J.; Gan, J.; Zhu, M.; Hu, Z.; Chu, J. Electronic structures and excitonic transitions in nanocrystalline iron-doped tin dioxide diluted magnetic semiconductor films: an optical spectroscopic study. Phys. Chem. Chem. Phys. 2011,13, 6211–6222.

(11) Li, P.; wen Zhang, C.; Lian, J.; Gao, S.; Wang, X. First-principles study on electronic and magnetic properties of Cu-doped CdS. Solid State Commun. 2011, 151, 1712 – 1715.

(12) Lamrani, A. F.; Belaiche, M.; Benyoussef, A.; Kenz, E. Electronic structures and ferromagnetism of SnO2 (rutile) doped with double-impurities: First-principles calculations. J. Appl. Phys. 2014, 115, 013910.

(13) Inpasalini, M. S.; Choubey, R. K.; Mukherjee, S. Evidence of Bound Magnetic PolaronMediated Weak Ferromagnetism in co-doped SnO2 Nanocrystals: Microstructural, Optical, Hyperfine, and Magnetic Investigations. J. Electron. Mater. 2016, 45, 3562–3569.

(14) Punnoose, A.; Hays, J.; Thurber, A.; Engelhard, M. H.; Kukkadapu, R. K.; Wang, C.; Shutthanandan, V.; Thevuthasan, S. Development of high-temperature ferromagnetism in SnO2 and paramagnetism in SnO by Fe doping. Phys. Rev. B 2005, 72, 054402.

(15) Wang, H.; Yan, Y.; Mohammed, Y.; Du, X.; Li, K.; Jin, H. First-principle study of magnetism in Co-doped SnO2. J. Magn. Magn. Mater. 2009, 321, 337 – 342.

(16) Coey, J.; Venkatesan, M.; Fitzgerald, C. Donor impurity band exchange in dilute ferromagnetic oxides. Nat. Mater. 2005, 4, 173.

(17) Chang, G. S.; Forrest, J.; Kurmaev, E. Z.; Morozovska, A. N.; Glinchuk, M. D.;McLeod, J. A.; Moewes, A.; Surkova, T. P.; Hong, N. H. Oxygen-vacancy-induced ferromagnetism in undoped

ISSN: 2366-1313

SnO2 thin films. Phys. Rev. B 2012, 85, 165319.

(18) Haverkort, M. W. Quanty for core level spectroscopy - excitons, resonances and band excitations in time and frequency domain. J. Phys.: Conf. Ser. 2016, 712, 012001.

(19) Green, R. J.; Boukhvalov, D. W.; Kurmaev, E. Z.; Finkelstein, L. D.; Ho, H. W.; Ruan, K. B.; Wang, L.; Moewes, A. Room-temperature ferromagnetism via unpaired 20 dopant electrons and p − p coupling in carbon-doped In2O3: Experiment and theory. Phys. Rev. B 2012, 86, 115212.

(20) Haverkort, M. W.; Sangiovanni, G.; Hansmann, P.; Toschi, A.; Lu, Y.; Macke, S. Bands, resonances, edge singularities and excitons in core level spectroscopy investigated within the dynamical mean-field theory. Eur. Phys. Lett. 2014, 108, 57004.

(21) Viswanatha, R.; Sapra, S.; Sen Gupta, S.; Satpati, B.; Satyam, P. V.; Dev, B. N.; Sarma, D. D. Synthesis and Characterization of Mn-Doped ZnO Nanocrystals. J. Phys. Chem. B 2004, 108, 6303–6310.